Pharmaceutical Research, Vol. 23, No. 11, November 2006 (© 2006)
DOI: 10.1007/s11095-006-9103-5

Expert Review

Real-time Imaging and Quantification of Brain Delivery of Liposomes

Michal T. Krauze,[1] John Forsayeth,[1] John W. Park,[3] and Krystof S. Bankiewicz[1,2,4]

Received March 24, 2006; accepted June 26, 2006; published online September 14, 2006

Abstract. The surgical delivery of therapeutic agents into the parenchyma of the brain is problematic because it has been virtually impossible to know with any certainty where infused material is going, and how much to infuse. We have started to use liposomes loaded with Gadoteridol (GDL) as a tracer that allows us to follow infusions in real-time on magnetic resonance imaging (MRI). MRI allows precise tracking and measurement of liposomes loaded with markers and therapeutics. This review provides an overview of real-time delivery of liposomes to the central nervous system (CNS), and discusses the technical aspects of delivery, liposomes as colloidal systems of delivery, real-time distribution of liposomes in CNS, and quantification of liposome distribution. Our data suggests that real-time monitoring of liposomal drug infusion is likely to improve outcomes of clinical trials where convection-enhanced delivery (CED) is being used to target drugs to specific brain structures through limitation of systemic toxicity and reduction of side effects. This review is a summary of work done by our group over the past four years.

KEY WORDS: blood–brain barrier; CED; convection-enhanced delivery; direct drug delivery; liposome; MR; MRI.

BACKGROUND

Drug delivery to human CNS has long posed a major challenge. Despite recent advances in pharmacology the blood–brain barrier (BBB) remains the limiting factor in delivery of therapeutics to the CNS. Less than 1% of systemically administered drugs reach the brain, regardless of the physical and chemical properties of the drug, and regardless of manipulations to increase capillary permeability. Because of limitations imposed by the BBB, many different methods have been explored to increase drug delivery to the brain, such as vector-mediated delivery (use of the transferrin receptor to open the BBB biochemically), intra-arterial chemotherapy, and hyperosmotic BBB disruption (1–3). In 1994, Bobo *et al.* introduced convection-enhanced delivery (CED) as a new way to direct drug delivery to CNS (4). This local infusion technique utilizes bulk flow to enable the delivery of small and large molecules to clinically significant volumes of targeted tissues, thereby offering improved volume of distribution (Vd) compared to simple diffusion. Several works have since been published concerning the physiological and physical properties governing the flow of convection-enhanced molecules in CNS (5–7). CED now is gaining clinical acceptance for applications in neuro-oncology (8–10) and neurodegenerative diseases (11,12).

Liposomes are nanoscale carriers that consist typically of a phospholipid membrane shell surrounding a hollow core that can be used to encapsulate small molecules. Recent advances with liposomes as pharmaceutical carriers have received a lot of attention as experimental applications have moved into clinically approved products. Liposomal anthracyclines represent the first successful examples of nanoparticle-based anticancer treatments, and are found in approved formulations such as pegylated liposomal doxorubicin (Doxil, Alza Pharmaceuticals; Caelyx, Schering-Plough) and liposomal daunorubicin (Daunoxome, Gilead) (13–16). Clinical trials have demonstrated improvement in survival in patients with breast-carcinoma metastases (17), squamous cell cancer of head and neck (18), and ovarian cancer (19). One of the disadvantages of systemic liposomes is their rapid elimination from the blood, and capture of the liposomal preparations by the cells of the reticulo-endothelial system (20). Currently, a number of efforts are underway to reduce this problem.

CED of liposomes to CNS has been explored to establish more efficient drug delivery to CNS. The significant advantage of this method is that liposomes are delivered directly to the region of interest without facing either the fast elimination seen in systemic application or the difficulties of penetrating the BBB with systemically delivered drug. In rodents, we have observed excellent distribution of liposomes containing fluorescent dye after CED into normal striatum, as well as into implanted brain tumor xenografts (21).

[1] Department of Neurological Surgery, Laboratory for Molecular Therapeutics, University of California San Francisco, San Francisco, California, USA.
[2] Department of Neurological Surgery, University of California, San Francisco, 1855 Folsom Street, Mission Center Building Room 226, San Francisco, California 94103, USA.
[3] Division of Hematology-Oncology, University of California San Francisco, San Francisco, California 94143, USA.
[4] To whom correspondence should be addressed. (e-mail: krystof.bankiewicz@ucsf.edu)

Further experiments with CED of liposomes led to development of a magnetic resonance (MR) real-time imaging method to track liposomes in which Gadoteridol is encapsulated (GDL) (22). We showed that CED of GDL is an excellent way to track distribution in various regions of the brain in real-time on MRI. Current studies aim to establish a clinically applicable real-time convective delivery of liposomes (23). Monitored CED in the significantly larger primate brain allowed us to address clinically relevant issues of safety, distribution and toxicity (23,24). In that study, MRI of GDL was highly predictive in the determination of liposomal tissue distribution, confirmed by histological comparison with concomitant administration of fluorescent liposomes. In addition, we have also shown that liposomal distribution stops immediately when delivery pumps are turned off. This is an important finding because it permits filling of specific brain regions with a known quantity of liposome, and thus of encapsulated drug, in a very controllable manner. However, it became clear in the course of these MRI studies that there are significant regional differences in the factors governing flow of interstitially infused substances within the CNS. Emerging therapeutic strategies for various diseases of the CNS warrant a better understanding of delivery and distribution within distinct brain areas. We used real-time MRI to infuse corona radiata, putamen and brainstem with 700 μl of liposomes and detected gross regional differences in liposomal distribution in primate brain. MR imaging is a powerful tool for monitoring real-time distribution of liposomes, and consequently for accurate calculation of Vd. Understanding the role of distribution pathways in the regulation of Vd in specific anatomic regions is important for current and future clinical applications of CED and liposomes. Our results show that Vd of liposomes is determined primarily by the anatomic structure targeted by CED.

CONSIDERATIONS IN METHOD DEVELOPMENT

Delivery Apparatus

The delivery catheter used in our CED studies is of great importance for the efficient distribution/ convection of the infused molecules. Morrison *et al.* developed a mathematical model that yielded a simple relationship between catheter diameter, volumetric inflow rate, and parameters that describe hydraulic flow through deformable tissue (25). This model showed that reduction of catheter needle diameter reduces backflow and reflux in rodent brain. It is crucial to avoid backflow and reflux when applying CED to CNS delivery since the drainage of fluid along needle shaft diminishes distribution greatly (26). Therefore, we developed a step-design cannula (Fig. 1) for CED that avoids backflow and reflux, and thus permits higher infusion rates without compromising on distribution volume (26). Maximum delivery speed was 0.5 μl/min through a simple 32-gauge catheter needle. However, in our primate studies we now routinely infuse liposomes at 3 μl/min with the improved device. The outer step in the design allows improved convection parameters at any speed when compared to standard catheter needles (Fig. 1A–D).

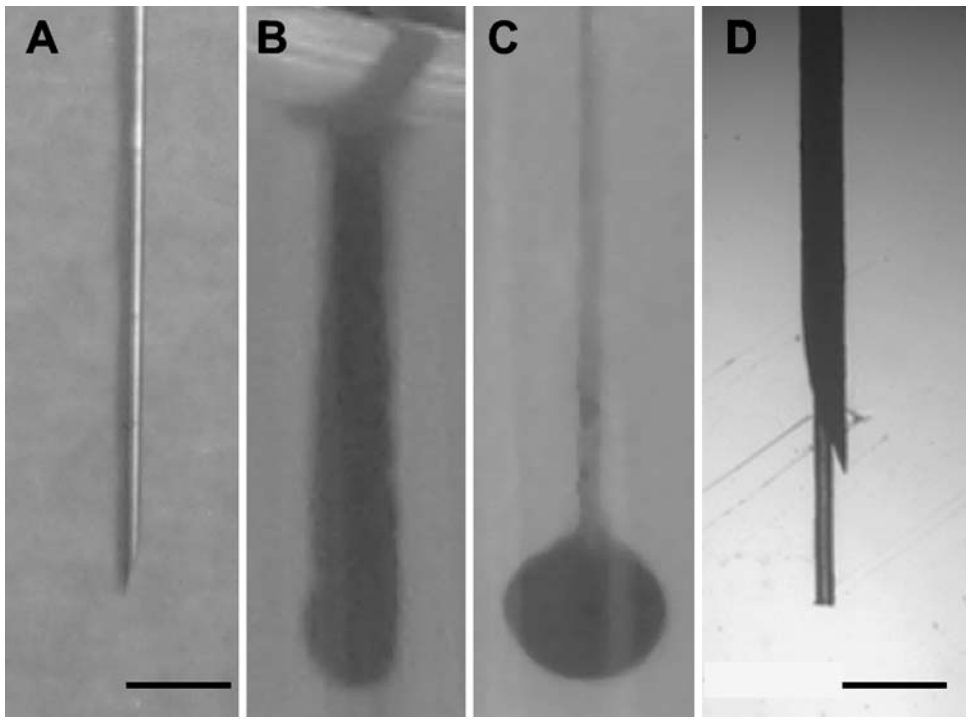

Fig. 1. Cannula types and resulting distribution in agarose gel. (A) 24-gauge needle; (B) reflux of trypan blue along needle-shaft of 24-gauge cannula in agarose gel at 1 μl/min; (C) improved distribution of trypan blue in agarose gel with step-design cannula at 1 μl/min; (D) step-design cannula consisting of a 24-gauge needle with glued in silica insert. [Scale in image (A) equals 1 cm, Scale in image (D) equals 1 mm]. This work was originally published in Krauze *et al.* (2005), ref (26).

Preparation of Loading Lines and Pumps

Sterile infusion catheters and loading lines are connected by means of the appropriate fittings with great care taken to eliminate air bubbles from the system. Oil infusion lines are prepared and 1-ml gas-tight Hamilton syringes is filled with oil and mounted onto a micro-infusion pump. After the union of the oil and loading lines (containing GDL), the infusion catheters are primed with GDL and the infusion system is transferred to the MRI. The main rate-controller of the infusion pumps is placed outside MRI room and connected via cable to the pumps to avoid electromagnetic interference from the MR magnets. Based on MRI coordinates, the catheter is mounted onto a stereotactic holder, and guided to the targeted regions of the brain through a guide-cannula previously secured [see (23) for details]. The length of each infusion catheter is measured to ensure that the distal tip extended approximately 3 to 4 mm beyond the length of the respective guide. This creates a stepped design at the tip of the cannula as described above. Initial infusion rates is set at 0.1 μl/min, the lines visually inspected to ensure a smooth flow of fluid through the system, and the catheters lowered to their target sites.

Liposomes

Liposomes that contain MRI contrast agent are composed of a mixture of phospholipid, cholesterol, and a pegylated phospholipid in a molar ratio of 3:2:0.3. The liposomes are neutral with respect to charge and stabilized by the presence of polyethylene glycol chains. The standard MRI contrast reagent, Gadoteridol, a chelated Gadolinium, is introduced into the lipid mixture before they are extruded as liposomes with a diameter of 124 ± 24.4 nm as determined by quasi-elastic light scattering [see (23) for detailed methods].

Distribution in brain of liposomes after convection-enhanced delivery is influenced by particle charge, particle diameter, and presence of a steric coating (27,28). Liposome contents are released by diffusion into the convected area of the CNS (21). This slow release drives a dramatic improvement in the pharmacokinetic properties of the encapsulated drug. Control of the tissue affinity of locally delivered liposomes can be used in addition to CED to optimize local distribution within the brain. As an example of how surface properties modulate distribution, we have shown differences in distribution of a mixture of pegylated (10% mol/mol) cationic liposomes with DiOC18 fluorescence (Fig. 2, upper) *versus* non-pegylated cationic liposomes with DiIC18 fluorescence (Fig. 2, lower). The presence of PEG on the surface presumably shields the positive charges on the liposomes that otherwise mediate avid binding to cells as soon as they leave the cannula (28). Another aspect of this shielding phenomenon is the effect of encapsulating molecules with strong tissue binding into liposomes. CED of the free doxorubicin is almost completely confined to the area of the needle tip due to its high nuclear affinity (Fig. 3A upper panel) of the chemotherapeutic, whereas liposomal doxorubicin distributes very well in the interstitial space (28) (Fig. 3A lower panel). The broader distribution of this chemotherapeutic agent is associated with increased efficacy in rodent tumor models, decreased toxicity, and longer tumor half-life (29,30).

Quantitation of Liposome-entrapped Gadoteridol by MRI

The concentration of Gadoteridol entrapped in the liposomes can be determined from nuclear MR relaxivity measurements. The relationship between the change in the intrinsic relaxation rate imposed by a paramagnetic agent (ΔR), also known as "T1 shortening," and the concentration of the agent is defined by the equation: $\Delta R = r_1$[agent], in which r_1 = relaxivity of the paramagnetic agent and $\Delta R = (1/T1_{observed} - 1/T1_{intrinsic})$. As Gadoteridol was encapsulated within the liposome, we corrected for the change in the observed T1 imposed by the lipid by measurement of the T1 of solubilized liposomes, with and without Gadoteridol, by means of an iterative inversion-recovery *MRI* sequence on a 2-Tesla Brucker Omega scanner (Brucker Medical, Karlsruhe, Germany). The relaxivity of Gadoteridol had been empirically derived previously on the same system and had a value of 4.07 $mM^{-1}s^{-1}$. The concentration of the encapsulated Gadoteridol was then calculated with the following equation: $[\text{Gadoteridol}] = [(1/T1_{wGado}) - (1/T1_{w/oGado})]/4.07$.

The concentration of Gadoteridol used in our studies ranged from 0.925−3.7 mM. Concentration studies (unpublished results) determined 0.925 mM to be the lowest concentration that could be used for volumetric calculations by our software. Defining the lowest calculable dose is important as future therapeutic applications may warrant the highest possible therapeutic liposome load at minimum GDL load.

MRI Acquisition

T1-weighted images of the primates' brains were acquired on a 1.5 Tesla Signa LX scanner (GE Medical Systems, Waukesha, WI) with a 5-in. surface coil. Prior to insertion of infusion catheters, baseline spoiled gradient echo (SPGR) images were taken: repetition time (TR)/echo time (TE)/flip angle = 28 ms/8 ms/40°, number of excitations (NEX) = 4, matrix = 256 × 192, field of view (FOV) = 16 cm×12 cm, slice thickness = 1 mm. These parameters resulted in a 0.391-mm^3 voxel volume. Once the catheters were inserted and the infusion commenced, SPGR scans were taken consecutively throughout the infusion. The scan time was dependent on the number of slices needed to cover the extent of infusion and ranged from 9 min 44 s to 11 min 53 s.

Distribution of Liposomes after Convection-enhanced Delivery Detected by Fluorescent Labeling

Our studies with convection-enhanced delivery were conducted first with fluorescent dye (rhodamine) loaded liposomes in rodent striatum. Excellent distribution was seen on fresh frozen sections taken immediately after an infusion of 20 - μl fluorescent liposome (Fig. 4A). In order to test the feasibility of CED of liposomes in a much larger non-human primate brain, liposomes loaded with fluorescent dye were infused by CED in a volume of 66 μl into the corona radiata (Fig. 4B) or putamen (Fig. 4C) of both hemispheres. The animals were euthanized immediately after the infusion

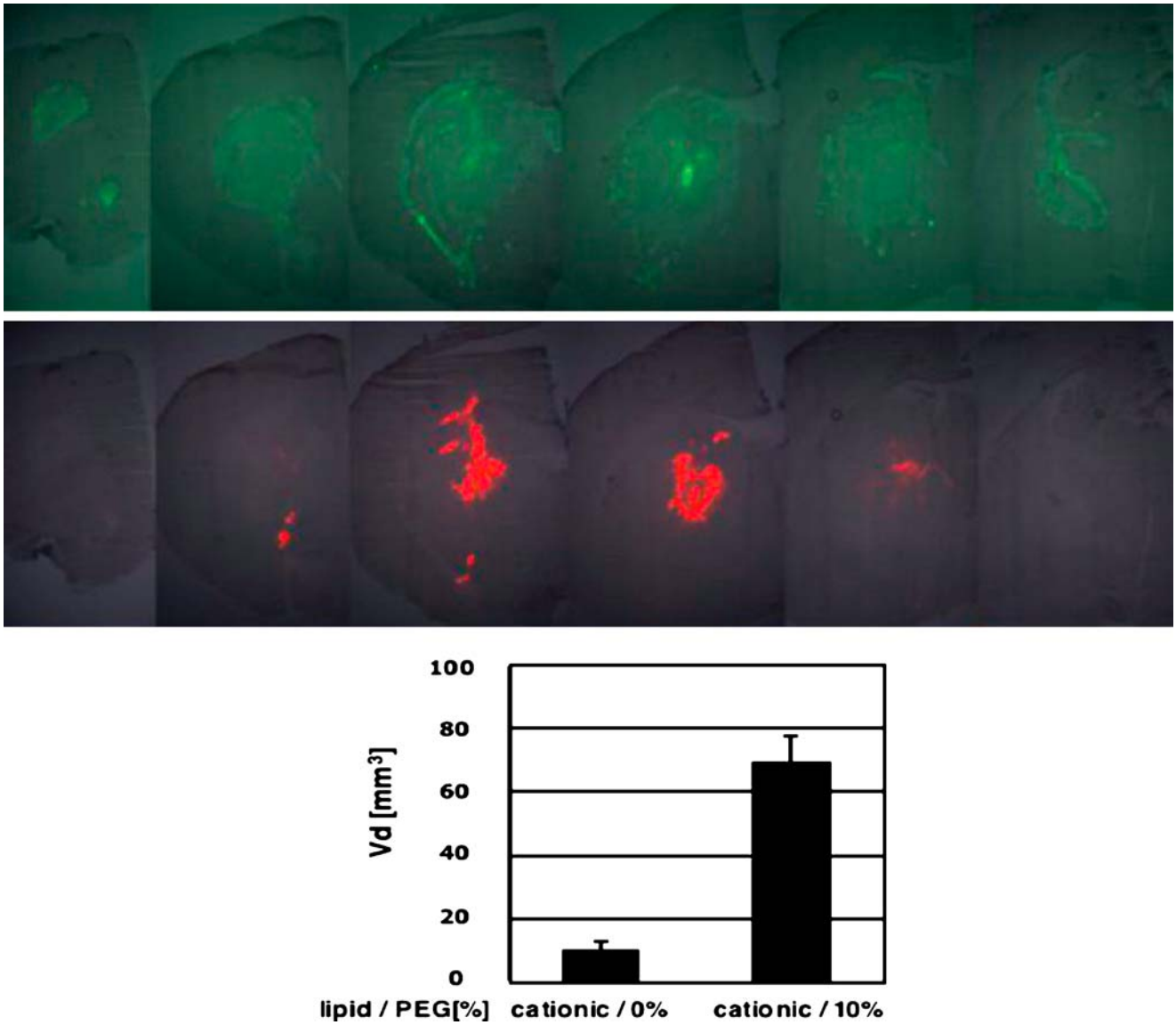

Fig. 2. Surface properties influence CED of liposomes in rodent CNS. Pegylation of cationic liposomes improves distribution in rodent striatum (*upper panel*) when compared with non-pegylated cationic liposomes (*lower panel*). Each panel represents rostral to caudal sections of rodent striatum. This figure was originally published in Saito *et al.* (2006), see (28).

procedure. A robust distribution of liposomes was achieved and was detected at necropsy (Fig. 4C), and also on histological sections (Fig. 4B).

Comparison of Fluorescent Distribution and MRI Distribution Real-time Monitoring of GDL Distribution in Putamen, Corona Radiata and Brain Stem

After establishing detection of GDL in rodent brains (22) we co-infused GDL with rhodamine-loaded liposomes in primate brain to assess whether histology and MRI data would yield the same distribution. Targeted infusion sites were the right corona radiata, the left putamen, and the left brain stem. Infusion volumes consisted of up to 113.5 µl for the corona radiata and putamen, and 66 µl for the brain stem. Robust and clearly delineated distributions of GDL were observed at each infusion site in the T1-weighted MR images obtained immediately after infusion. Comparison of MRI scans taken at the end of an infusion procedure were compared with post mortem fluorescent histology that revealed same area of distribution by histology and MRI (Fig. 5). Histological sections and MRI data were analyzed separately for distribution volume and plotted on a graph (see Fig. 9).

Magnet Resonance Imaging of GDL during CED in Primate Brain

During CED of GDL in primate brain, different distribution patterns and volumes were seen that depended on the region infused. The maximum volume of infusion (Vi) at each location was 700 µl. The lowest distribution volume (Vd) was seen in putamen yielding about 0.684 cm^3 after an infusion of 700 µl (Vi) that translates into a ratio of volume of infusion Vi/Vd of 1:1. Distribution in putamen was not only confined to the structure, because some movement of

liposomes into the medial cerebral artery of the infused side could be seen (Fig. 6). The perivascular space was previously only known to transport physiologic compounds within the brain. The liposomal signal of the MCA extending into the Sylvian fissure clearly showed the function of the perivascular space also for directly infused liposomes (31). The double perivascular space layer of basal ganglia arteries seems to allow transport against the flow of blood, whereas the single perivascular layer of the large cerebral arteries allows transport with the flow of blood. We are investigating this perivascular distributive mechanism further, and have recently described (32) in more detail various factors, such as blood pressure, in modifying the movement of nanoparticles through the parenchyma by means of this rather underappreciated mechanism.

Better distribution was seen in corona radiata where a 700-μl infusion translated into about 1 cm^3 of distribution volume, a Vi/Vd ratio of 1:1.4. Interestingly, distribution was confined to the white matter, and this resulted in the crossing of liposomes into the contralateral hemisphere via the white matter tracts of the corpus callosum (Fig. 7).

The best distribution in primate CNS of GDL was seen in brain stem where an infusion of 700 μl yielded a Vi of 1.6 cm^3, translating into a Vi/Vd ratio of 1:2.3 (Fig. 8) (28). The targeted area in all experimental subjects was the upper pons region. The distribution was mainly caudal as GDL moved towards the

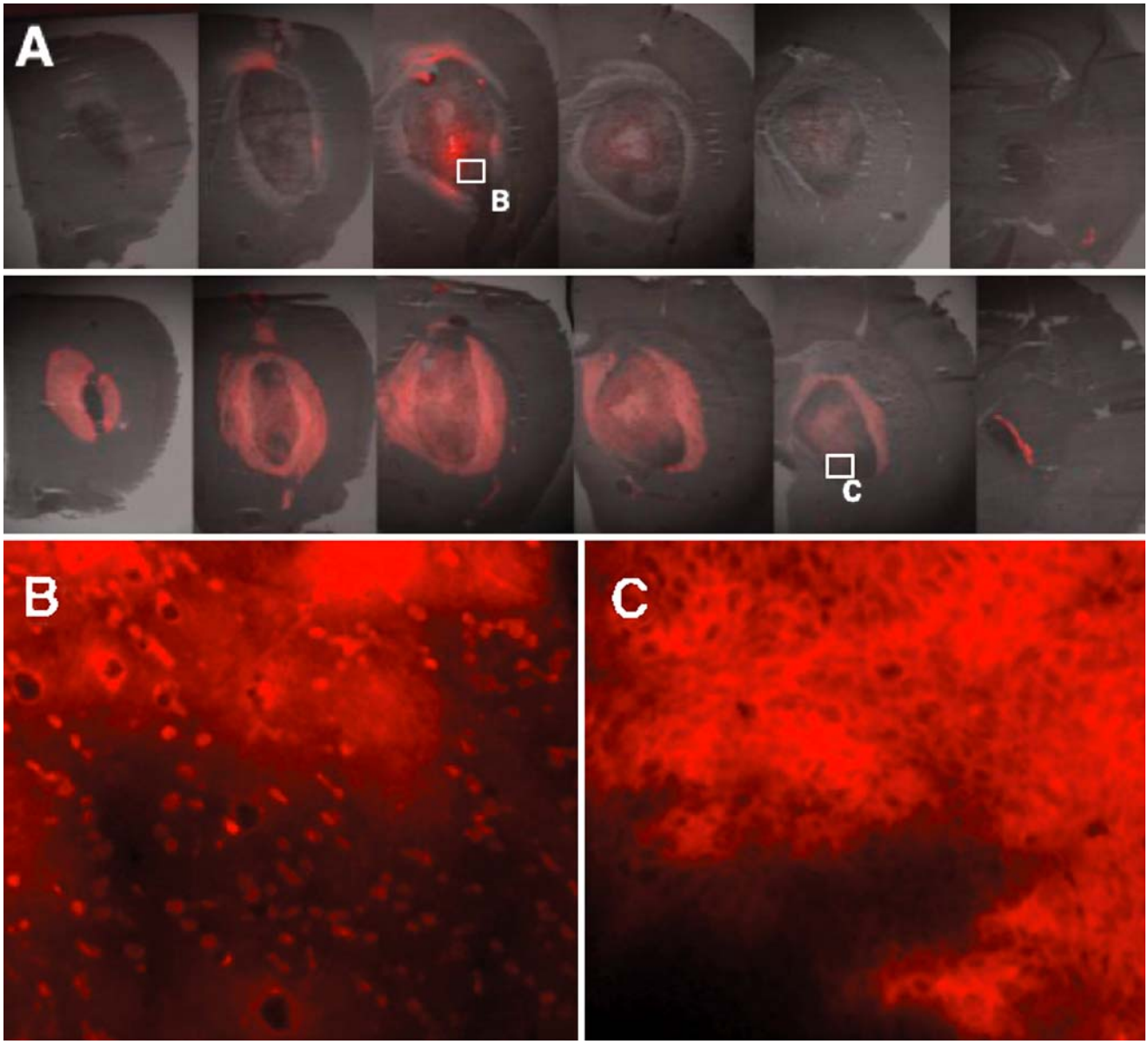

Fig. 3. CED of Doxorubicin and Liposomal Doxorubicin in rodent brain tumor xenografts. (A)*Upper panel* shows marginal distribution of doxorubicin that is confined to the injection site. *Lower panel* shows extensive distribution of liposomal doxorubicin. Each panel represents rostral to caudal sections of implanted intracranial tumor xenograft. (B) Free doxorubicin is mainly entrapped in cell nuclei, (C) whereas liposomal doxorubicin is distributed freely in the interstitial space, thereby covering the entire tumor mass. This figure was originally published in Saito *et al.* (2006), see (28).

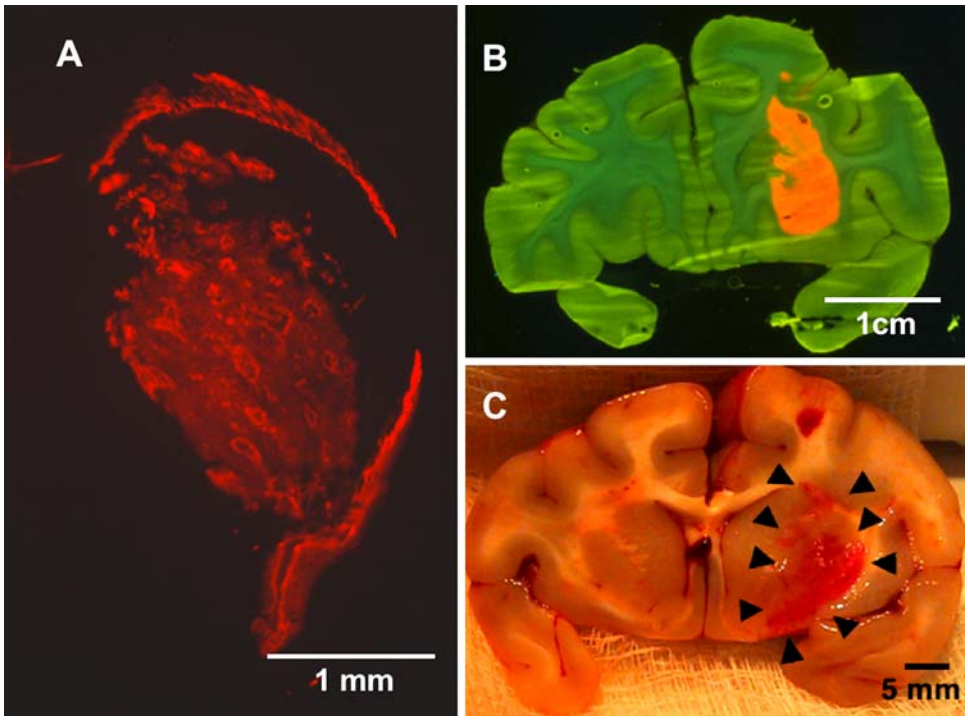

Fig. 4. Extensive distribution of fluorescent liposomes in CNS. (A) Almost complete coverage of rodent striatum by a 20-μl liposome infusion; (B) distribution visualized by UV light in primate putamen after 66-μl infusion; (C) view of liposome distribution in putamen immediately after infusion procedure.

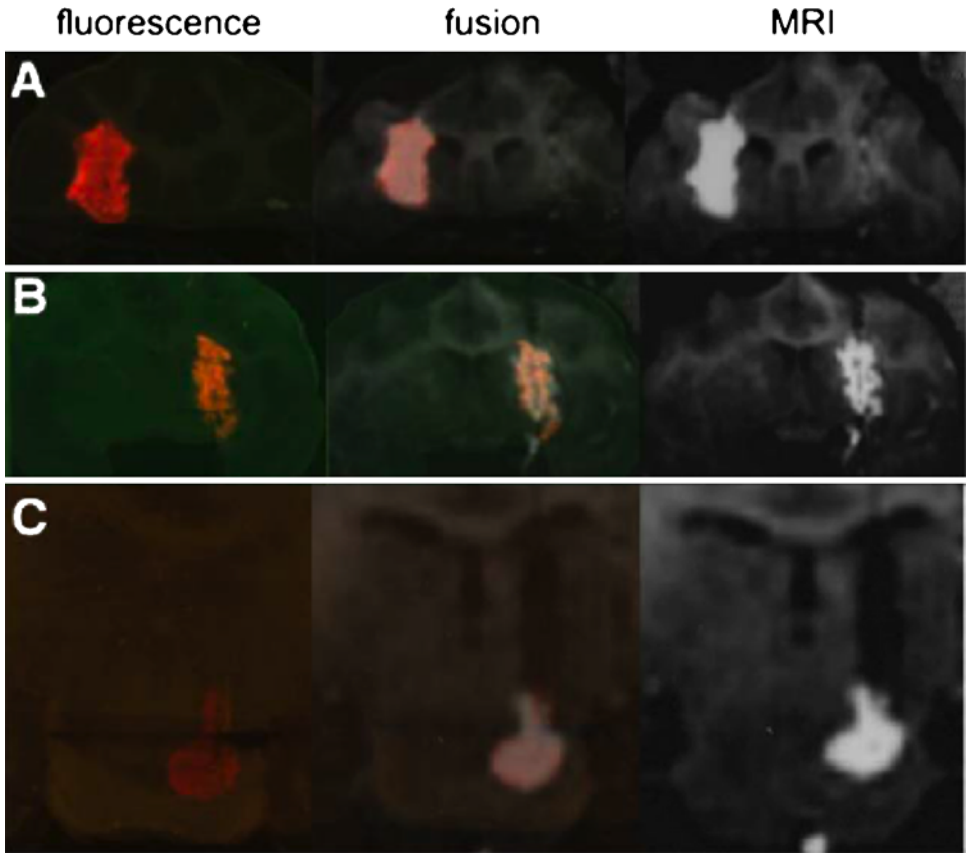

Fig. 5. Co-infused fluorescent liposomes overlap with GDL images from MR. Corona radiata (A), putamen (B) and brain stem (C) showed the same distribution area on *post mortem* histology when compared with *in vivo* MR data. All volumetric data gathered was later plotted graphically (see Fig. 9). This figure was originally published in Saito *et al.* (2005), see (23).

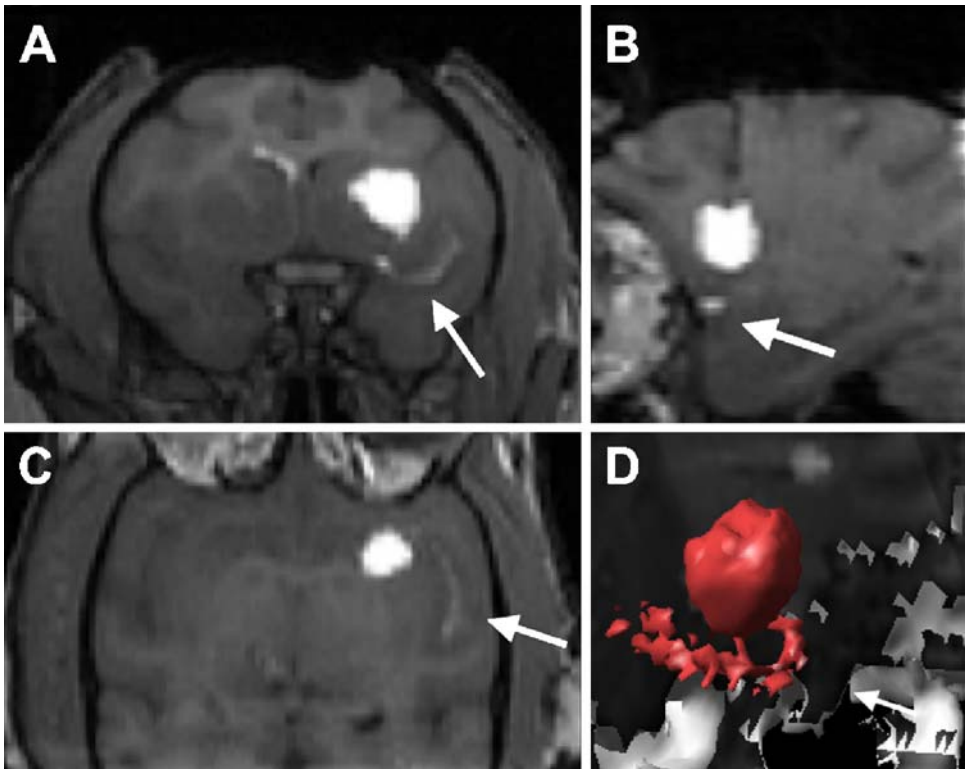

Fig. 6. CED of GDL in putamen. Distribution of GDL in putamen is shown in coronal (A), sagittal (B) and axial (C) views. Perivascular transport of GDL is seen during CED on MR via ipsilateral medial cerebral artery (MCA) from putamen infusion site (*white arrow* A – C). Three-dimensional reconstruction of a 300-μl infusion and perivascular transport pathway starting in lateral striate arteries going to the Sylvian fissure branches of the MCA.

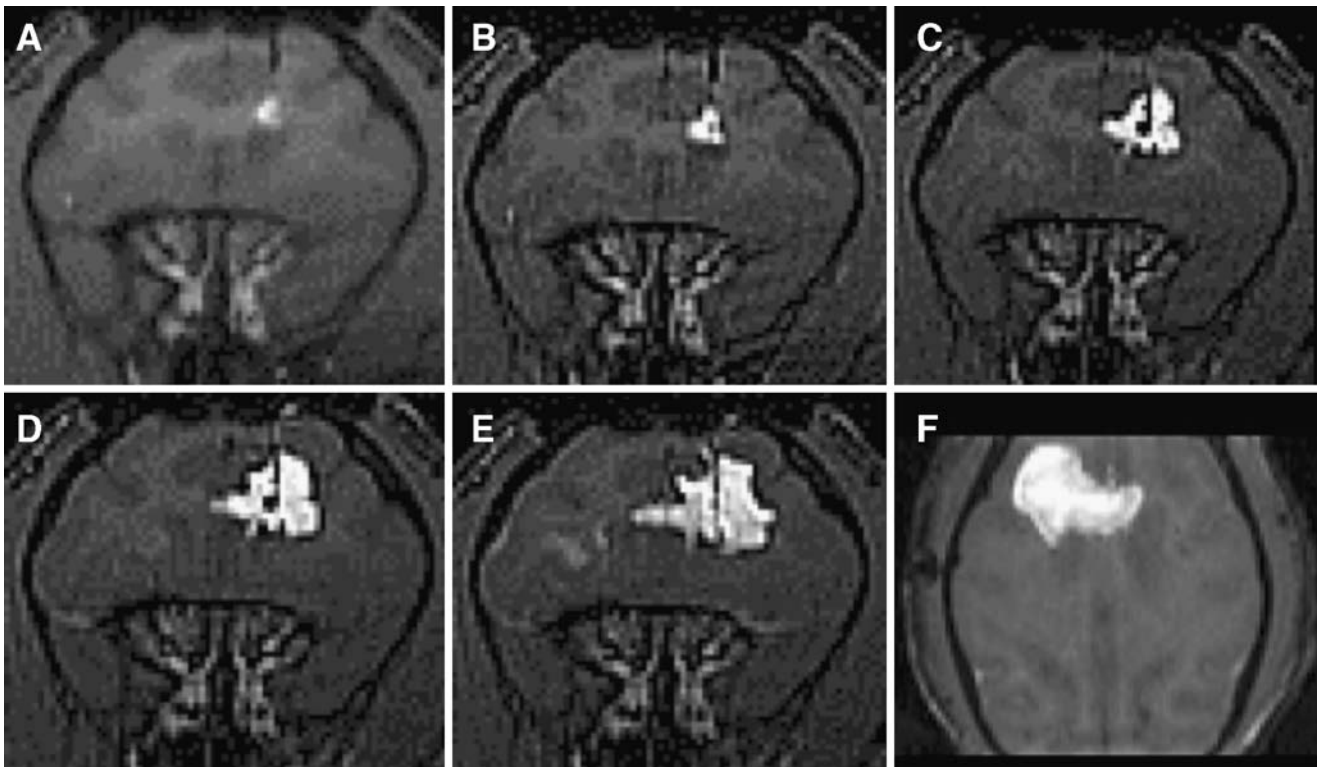

Fig. 7. Distribution of GDL in corona radiata. Distribution of GDL is shown in coronal (A – E) and axial views (F). Barely visible at 5 μl (A), GDL begin to cross into contralateral hemisphere from 500 μl on to 700 μl (D – F). Distribution stays almost confined to white matter. This figure was originally published in Krauze *et al.* (2005), see (24).

medulla oblongata that resulted in an almost complete coverage of the brain stem. In addition, GDL were observed to enter the cerebellum via the superior cerebellar peduncle. It is important to note that delivery of drugs into brain stem has long been known to be a difficult problem per se. Thus it was especially gratifying to see such effective distribution into this region.

Quantification of Distribution from MRI and Histology

Volume Quantitation from Fluorescent Images

After necropsy, animals' brains were sectioned on a cryostat. Sequential sections with 40-μm sections at 400-μm intervals were obtained. Rhodamine fluorescence was visualized using an ultraviolet light source, and a charged-coupled device camera with a fixed aperture was used to capture the images. The volume of fluorescent liposome distribution was analyzed on a Macintosh-based image analysis system (NIH Image 1.62; NIH, Bethesda, MD) as described previously (33).

Volume Quantification from MR Images

The volume of liposomal distribution within each infused brain region was quantified with BrainLab® software (Heimstetten, Germany). MR images acquired

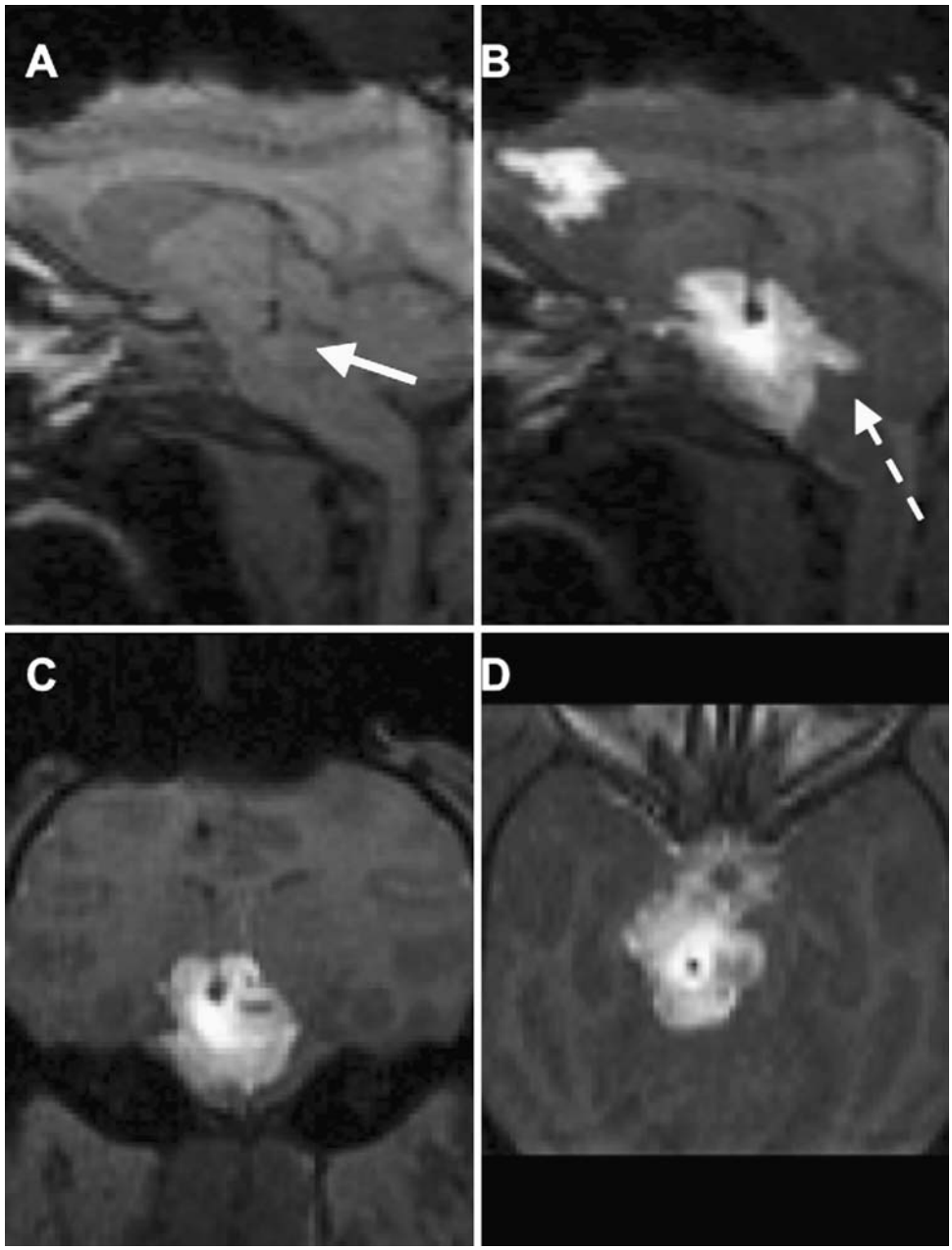

Fig. 8. Catheter placement in brain stem GDL infusion (A—white arrow). Distribution in brain stem seen after CED of 700 μl GDL in sagittal (B), coronal (C) and axial (D) views. (B) Sagittal view shows the strong caudal movement with respect to the infusion site, starting distribution into cerebellum (*dashed arrow*) and also concomitant corona radiata infusion.

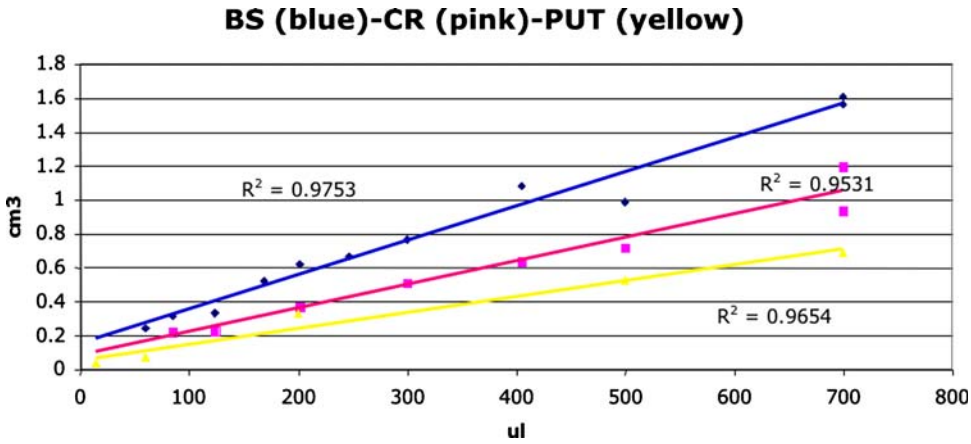

Fig. 9. Relationship between Vi (μl) and Vd (cm^3) of GDL in primate CNS. Data from histology analysis and MRI analysis was combined in this graph. Linear correlation of distribution is seen in each structure: brain stem (*blue*), corona radiata (*pink*) and putamen (*yellow*). A strong linear correlation (R^2) between Vd and Vi at all infusions was observed for each region. This figure was originally published in Krauze *et al.* (2005), see (24).

during the infusion procedure were correlated with volume of infusion in each series. BrainLab software reads all data specifications from MR images. After the pixel threshold value for liposomal signal is defined, the software calculates the signal above a defined threshold value and establishes the volume of distribution from primate brain. This allows volume of distribution to be determined at any given time point. Volumetric data gained from histology and MR analysis was plotted on one graph (Fig. 9). The graph shows the linear correlation for each infusion gained from infusion of several animals. No significant difference of distribution in anatomic structures infused was seen among the various primates infused and number of infusions performed in one primate. Also volumetric data obtained from histology and MR showed no significant difference. Data gained from MR analysis can be also used to create a three dimensional reconstruction in order to create an anatomic relationship to the entire animal head (Fig. 10).

Potential Clinical Applications

Patients affected by malignant brain tumors usually benefit only slightly from systemic chemotherapy or surgical removal of tumor. Experiments with CED of liposomes loaded with the chemotherapeutic CPT-11 to rodent intracranial brain tumor xenografts have shown excellent pharmacokinetic properties (Fig. 11). The unencapsulated drug was cleared within hours from the brain, whereas the liposomal form of the same concentration was detectable over 12 days. The highest load of CPT-11 into liposomes allows an extremely prolonged release in brain after CED, and drug was detectable for more than 50 days after a single application. This slow release resulted also in very beneficial toxicity profiles of liposomes (Fig. 12). CED of increasing doses of free CPT-11 to rodent brain showed high toxicity at relatively low doses (Fig. 12A, B). However, liposomal CPT-11 showed no toxicity at the current technical maximal load of 80 mg/ml corresponding to 1.6 mg in a 20-μl infusion. These very

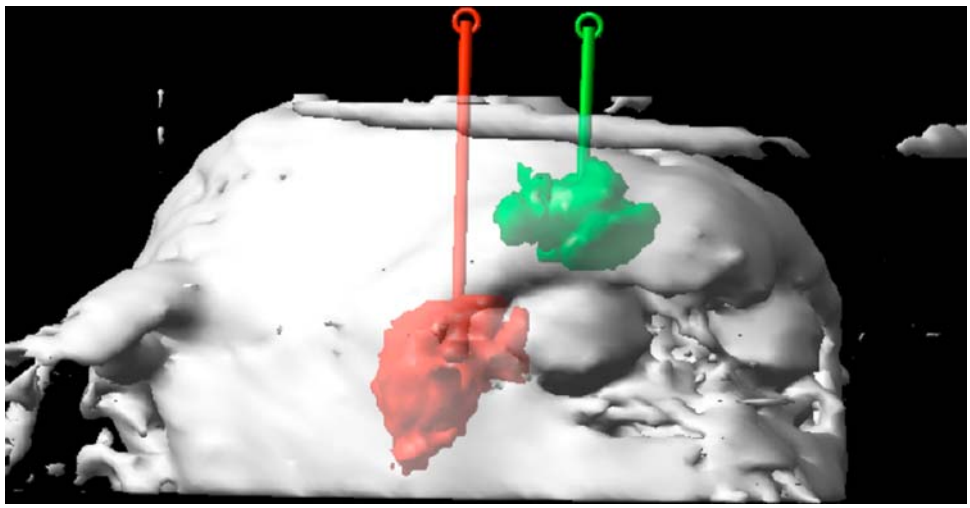

Fig. 10. Three-dimensional reconstruction of primate GDL infusion. Three-dimensional reconstruction of Vd demonstrates the relationship between GDL infusion and brain structures, and also allows volumetric measurements (see Fig. 9). Future applications are likely to use this feature for planning purposes of distribution *in vivo*.

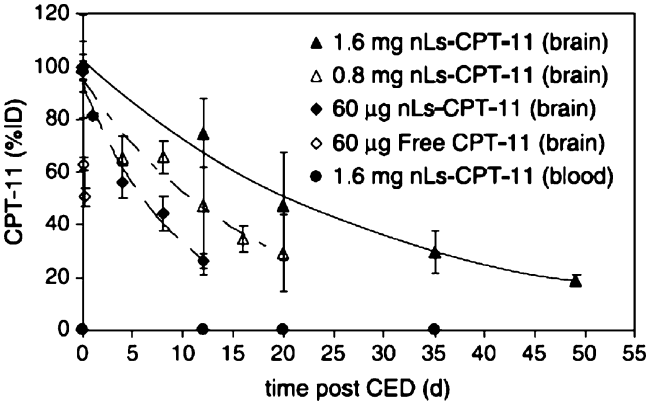

Fig. 11. Pharmacokinetics of free CPT-11 and liposomal (nLs) CPT-11 in the normal adult rat brain and blood after CED infusion. All values are % initial dose (ID) after CED of 20 µl of infusate. Drug concentrations were determined by HPLC assay for CPT-11/HCl. CPT-11 concentrations in blood were all below the detection limit of 1 ng/ml (0.03% ID). This figure was originally published in Noble *et al.* (2006), see (30).

promising pharmacologic findings translated into eradication or dramatically prolonged survival of rodents bearing intracranial U87 xenografts (Fig. 13) (30). Although no great difference was seen in low-dose free CPT-11 (Fig. 13d) *versus* low dose Ls-CPT-11 (Fig. 13c), the fact that high-dose Ls-CPT-11 could be used in the absence of limiting brain toxicity suggests a direct clinical application of this technology to the treatment of brain tumors.

CONCLUSION

The direct delivery of drugs into brain is gaining in popularity. By overcoming the blood–brain barrier and rapid

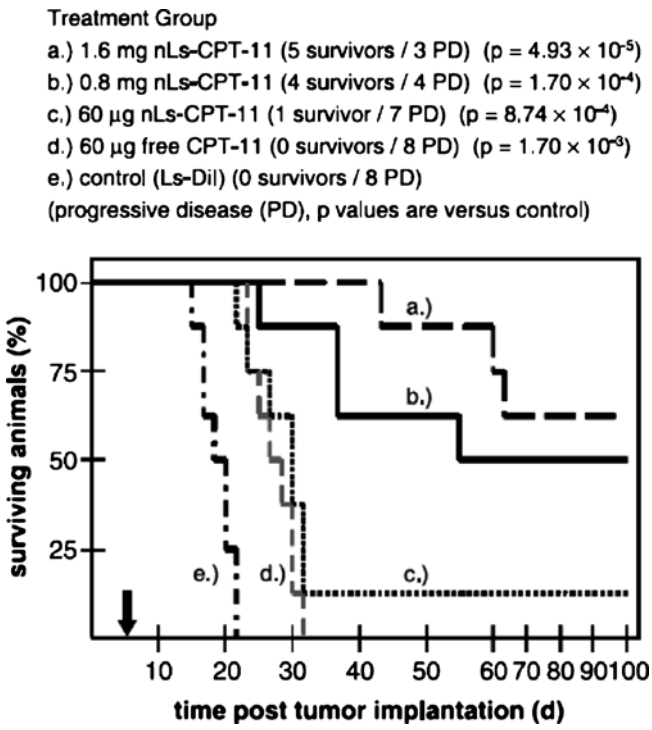

Fig. 13. Treatment of rats bearing orthotopic U87 tumors with single CED infusion of free or liposomal CPT-11. Five days after tumor implantation within the brain (*arrow*), rats were treated with liposomal CPT-11 at a) 1,600 µg (80 mg/ml), (b) liposomal CPT-11 at 800 µg (40 mg/ml), (c) liposomal CPT-11 at 60 µg (3 mg/ml), (d) free CPT-11 at 60 µg (3 mg/ml), and (E) liposomal DiIC18(3) without encapsulated drug (empty liposomes). Eight animals per group were used. Median survival for each group was (a) >100 days, (b) 78 days, (c) 30 days, (d) 28.5 days, and (e) 19.5 days. This figure was originally published in Noble *et al.* (2006), see (30).

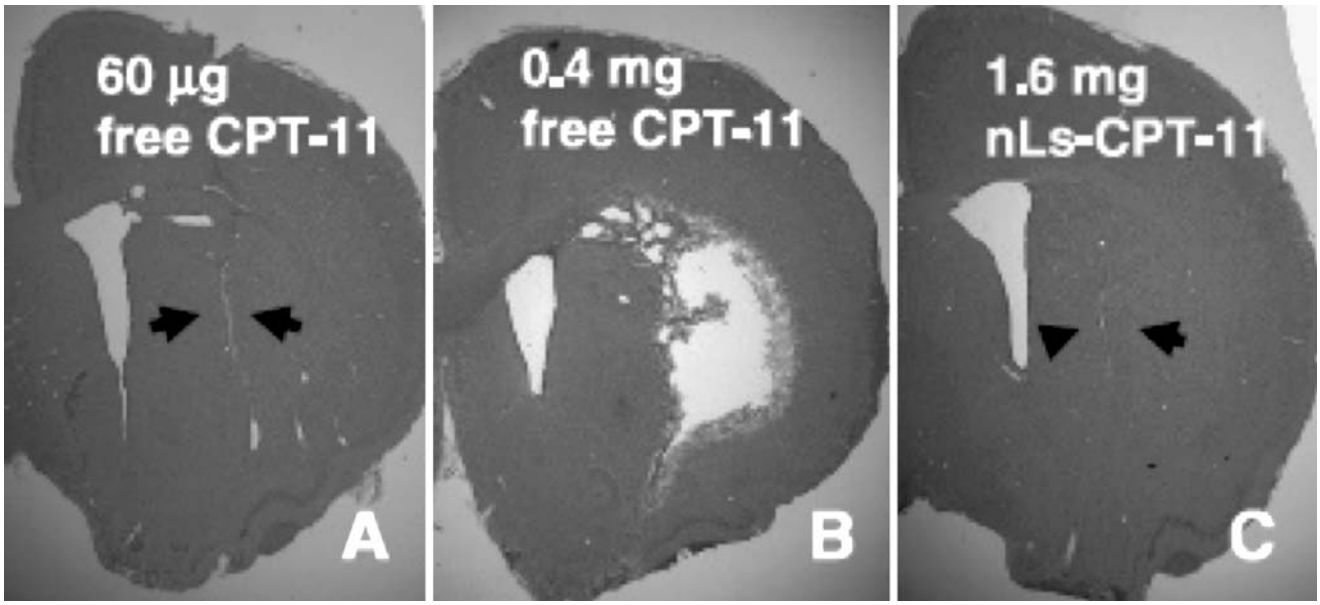

Fig. 12. Tissue toxicity of free CPT-11 and liposomal CPT-11 in the normal adult rat brain after CED. Rats (n = 4 per condition) were infused by CED with 20-µl volumes of drug or liposome. (A) free CPT-11 at 60 mg (3 mg/ml); (B) free CPT-11 at 0.4 mg (20 mg/ml). (C) liposomal CPT-11 at 1.6 mg (80 mg/ml). Six weeks later, animals were sacrificed and brains were processed for histopathology. Shown in each panel are representative H&E sections from each group. Extensive tissue injury was observed in all animals treated with 0.4 mg free CPT-11. Rats in other treatment groups showed only focal traumatic injury (*arrows*) at the site of the infusion cannula. This figure was originally published in Noble *et al.* (2006), see (30).

Tsystemic elimination of therapeutics, CED offers tremendous potential for the treatment of CNS pathologies. However, current clinical trials using sub-optimal delivery methods, i.e., the drugs are being infused into locations and at rates that are usually based on criteria such as location of the target in relation to sulci and ventricular structures, and not on an understanding of the physiological aspects of drug delivery. Even side effects seen in these trials are difficult to explain as no monitoring technique during delivery is used. Results gained in our rodent and primate experiments through the visualization of distribution in CNS have opened new vistas in CED. The step-design catheter especially designed for CED ensures not only a reflux-free, but also targeted, delivery to a predetermined area. Possible "spill-over" into neighboring structures or can be stopped immediately by simply turning off the infusion pump. Liposomes are already known to be extremely versatile nano-particles and have shown excellent distribution in our studies. By mixing GDL with therapeutic (drug-loaded) liposomes, it is now possible to customize drug delivery to the individual CNS in a way that enhances efficacy and limits toxicity. This would likely not only improve safety of delivery but also introduce the feature of slow therapeutic release from liposome found in our rodent studies. Slow but constant release of therapeutics from liposomes was both less toxic compared to the free drug and more efficacious in rodent brain tumor xenografts (30). Another important aspect is the linear distribution of liposomes in CNS that is influenced by the cyto-architecture of the brain anatomy. This makes any delivery highly predictable and calculable with computer software. Data acquired from MRI of liposome distribution is highly accurate as shown in our studies. Further development should eliminate current inter-rater variability that results from manual threshold definition. Applications of real-time CED could be simulated on computer before actual delivery in order to calculate dose and risks involved in a particular procedure. One might speculate that drugs previously deemed unacceptable for the treatment of brain diseases either for kinetic reasons or for systemic toxicity might be resurrected if compatible with this liposomal delivery technology.

We envisage the first clinical application of our real-time imaging technique to be in the field of neuro-oncology. We have amply demonstrated a sharp improvement in rat tumor models. We have more recently take the next step towards clinical translation has been achieved by treatment of spontaneous brain tumors in dogs that present much more like human glioblastomas. We have now performed targeted delivery of a GDL/Ls-CPT-11 mix into a canine brain tumor (grade III astrocytoma), and plan to undertake more such infusions as part of a veterinary medicine program in canine brain tumors at the University of California Davis, School of Veterinary Medicine. As larger brains will likely need more than one catheter in order to cover the entire tumor mass, we hope to define in our current canine studies optimal catheter placement parameters that will allow optimal distribution through multiple catheters in the larger brain setting.

Although still not well explored, neurodegenerative diseases like Parkinson are also likely to benefit from real-time delivery. Clinical trials that use CED of glial-derived neurotrophic factor (GDNF) are also likely to benefit by combining GDNF, GDL and imaging (11,12). As liposomes gain more and more attention for all clinical applications, we expect to see additional innovations that will further broaden our understanding of CED of liposomes in CNS.

ACKNOWLEDGMENTS

Special thanks to BrainLAB for support and help with iPlan® software, and to Hermes Biosciences for the generous supply of liposomes.

REFERENCES

1. C. H. Hsieh, Y. F. Chen, F. D. Chen, J. J. Hwang, J. C. Chen *et al*. Evaluation of pharmacokinetics of 4-borono-2-(18)F-fluoro-L-phenylalanine for boron neutron capture therapy in a glioma-bearing rat model with hyperosmolar blood–brain barrier disruption. *J. Nucl. Med.* **46**(11):1858–1865 (2005).
2. A. Weyerbrock, S. Walbridge, R. M. Pluta, J. E. Saavedra, L. K. Keefer *et al*. Selective opening of the blood–tumor barrier by a nitric oxide donor and long-term survival in rats with C6 gliomas. *J. Neurosurg.* **99**(4):728–737 (2003).
3. Y. Zhang, W. M. Pardridge *et al*. Delivery of beta-galactosidase to mouse brain via the blood–brain barrier transferrin receptor. *J. Pharmacol. Exp. Ther.* **313**(3):1075–1081 (2005).
4. R. H. Bobo, D. W. Laske, A. Akbasak, P. F. Morrison, R. L. Dedrick *et al*. Convection-enhanced delivery of macromolecules in the brain. *Proc. Natl. Acad. Sci. U. S. A.* **91**(6):2076–2080 (1994).
5. M. Y. Chen, R. R. Lonser, P. F. Morrison, L. S. Governale, and E. H. Oldfield. Variables affecting convection-enhanced delivery to the striatum: a systematic examination of rate of infusion, cannula size, infusate concentration, and tissue-cannula sealing time. *J. Neurosurg.* **90**(2):315–320 (1999).
6. D. W. Laske, P. F. Morrison, D. M. Lieberman, M. E. Corthesy, J. C. Reynolds *et al*. Chronic interstitial infusion of protein to primate brain: determination of drug distribution and clearance with single-photon emission computerized tomography imaging. *J. Neurosurg.* **87**(4):586–594 (1997).
7. P. F. Morrison, D. W. Laske, H. Bobo, E. H. Oldfield, and R. L. Dedrick. High-flow microinfusion: tissue penetration and pharmacodynamics. *Am. J. Physiol.* **266**(1 Pt 2):R292–R305 (1994).
8. S. Kunwar. Convection enhanced delivery of IL13-PE38QQR for treatment of recurrent malignant glioma: presentation of interim findings from ongoing phase 1 studies. *Acta Neurochir., Suppl.* **88**:105–111 (2003).
9. Z. Lidar, Y. Mardor, T. Jonas, R. Pfeffer, M. Faibel *et al*. Convection-enhanced delivery of paclitaxel for the treatment of recurrent malignant glioma: a phase I/II clinical study. *J. Neurosurg.* **100**(3):472–479 (2004).
10. Y. Mardor, O. Rahav, Y. Zauberman, Z. Lidar, A. Ocherashvilli *et al*. Convection-enhanced drug delivery: increased efficacy and magnetic resonance image monitoring. *Cancer Res.* **65**(15): 6858–6863 (2005).
11. S. S. Gill, N. K. Patel, G. R. Hotton, K. O'Sullivan, R. McCarter *et al*. Direct brain infusion of glial cell line-derived neurotrophic factor in Parkinson disease. *Nat. Med.* **9**(5):589–595 (2003).
12. N. K. Patel, M. Bunnage, P. Plaha, C. N. Svendsen, P. Heywood *et al*. Intraputamenal infusion of glial cell line-derived neurotrophic factor in PD: a two-year outcome study. *Ann. Neurol.* **57**(2):298–302 (2005).
13. A. A. Gabizon. Liposomal anthracyclines. *Hematol./Oncol. Clin. North Am.* **8**(2):431–450 (1994).
14. A. Gabizon, R. Isacson, E. Libson, B. Kaufman, B. Uziely *et al*. Clinical studies of liposome-encapsulated doxorubicin. *Acta Oncol.* **33**(7):779–786 (1994).
15. M. Zucchetti, A. Boiardi, A. Silvani, I. Parisi, S. Piccolrovazzi *et al*. Distribution of daunorubicin and daunorubicinol in human

glioma tumors after administration of liposomal daunorubicin. *Cancer Chemother. Pharmacol.* **44**(2):173–176 (1999).
16. J. T. Thigpen, C. A. Aghajanian, D. S. Alberts, S. M. Campos, A. N. Gordon *et al.* Role of pegylated liposomal doxorubicin in ovarian cancer. *Gynecol. Oncol.* **96**(1):10–18 (2005).
17. J. A. O'Shaughnessy. Pegylated liposomal doxorubicin in the treatment of breast cancer. *Clin. Breast Cancer* **4**(5):318–328 (2003).
18. K. J. Harrington, C. Lewanski, A. D. Northcote, J. Whittaker, A. M. Peters *et al*. Phase II study of pegylated liposomal doxorubicin (Caelyx) as induction chemotherapy for patients with squamous cell cancer of the head and neck. *Eur. J. Cancer* **37**(16):2015–2022 (2001).
19. S. R. Johnston and M. E. Gore. Caelyx: phase II studies in ovarian cancer. *Eur. J. Cancer* **37**(Suppl 9):S8–S14 (2001).
20. V. P. Torchilin. Recent advances with liposomes as pharmaceutical carriers. *Nat. Rev. Drug Discov.* **4**(2):145–160 (2005).
21. C. Mamot, J. B. Nguyen, M. Pourdehnad, P. Hadaczek, R. Saito *et al.* Extensive distribution of liposomes in rodent brains and brain tumors following convection-enhanced delivery. *J. Neuro oncol.* **68**(1):1–9 (2004).
22. R. Saito, J. R. Bringas, T. R. McKnight, M. F. Wendland, C. Mamot *et al*. Distribution of liposomes into brain and rat brain tumor models by convection-enhanced delivery monitored with magnetic resonance imaging. *Cancer Res.* **64**(7):2572–2579 (2004).
23. R. Saito, M. T. Krauze, J. R. Bringas, C. Noble, T. R. McKnight *et al*. Gadolinium-loaded liposomes allow for real-time magnetic resonance imaging of convection-enhanced delivery in the primate brain. *Exp. Neurol.* **196**(2):381–389 (2005).
24. M. T. Krauze, T. R. McKnight, Y. Yamashita, J. Bringas, C. O. Noble *et al.* Real-time visualization and characterization of liposomal delivery into the monkey brain by magnetic resonance imaging. *Brain Res. Protoc.* **16**(1–3):20–26 (2005).
25. P. F. Morrison, M. Y. Chen, R. S. Chadwick, R. R. Lonser, and E. H. Oldfield. Focal delivery during direct infusion to brain: role of flow rate, catheter diameter, and tissue mechanics. *Am. J. Physiol.* **277**(4 Pt 2):R1218–R1229 (1999).
26. M. T. Krauze, R. Saito, C. Noble, M. Tamas, J. Bringas *et al*. Reflux-free cannula for convection-enhanced high-speed delivery of therapeutic agents. *J. Neurosurg.* **103**(5):923–929 (2005).
27. J. A. MacKay, D. F. Deen, and F. C. Szoka Jr. Distribution in brain of liposomes after convection enhanced delivery; modulation by particle charge, particle diameter, and presence of steric coating. *Brain Res.* **1035**(2):139–153 (2005).
28. R. Saito, M. T. Krauze, C. O. Noble, M. Tamas, and D. C. Drummond *et al*. Tissue affinity of the infusate affects the distribution volume during convection-enhanced delivery into rodent brains: Implications for local drug delivery. *J. Neurosci. Methods* **154**(1–2):225–232 (2006).
29. R. S. R. Yamashita, M. T. Krauze, C. O. Noble, T. Kawaguchi, and K. S. Bankiewicz. Convection-enhanced delivery of liposomal doxorubicin in intracranial brain tumor xenografts. *Targeted-Oncology* (2006) in press.
30. C. O. Noble, M. T. Krauze, D. C. Drummond, Y. Yamashita, R. Saito *et al*. Novel Nanoliposomal CPT-11 infused by convection-enhanced delivery in intracranial tumors: Pharmacology and efficacy. *Cancer Res.* **66**(5):2801–2806 (2006).
31. M. T. Krauze, R. Saito, C. Noble, J. Bringas, J. Forsayeth *et al*. Effects of the perivascular space on convection-enhanced delivery of liposomes in primate putamen. *Exp. Neurol.* **196**(1): 104–111 (2005).
32. P. Hadaczek, Y. Yamashita, M. Mirek, and K. S. Bankiewicz. The "perivascular pump" driven by arterial pulsation is a powerful mechanism for the distribution of therapeutic molecules within the brain. *Molec. Ther.* **14**(1):69–78 (2006).
33. J. F. Hamilton, P. F. Morrison, M. Y. Chen, J. Harvey-White, R. S. Pernaute *et al*. Heparin coinfusion during convection-enhanced delivery (CED) increases the distribution of the glial-derived neurotrophic factor (GDNF) ligand family in rat striatum and enhances the pharmacological activity of neurturin. *Exp. Neurol.* **168**(1):155–161 (2001).